

Low-order modeling of non-premixed flames subjected to a transverse acoustic mode

By D. Brouzet AND M. Ihme

1. Motivation and objectives

Combustion instabilities (CIs) are one of the major challenges for the design and operation of gas turbines and rocket engines (Lieuwen & Yang 2005). These instabilities are characterized by large self-sustaining oscillations in pressure and heat release, arising from the coupling between combustion, acoustics, and unsteady flow field. While some papers examined CIs in annular combustors to study the nature of transverse modes (Wolf *et al.* 2012; Prieur *et al.* 2017; Rouwenhorst *et al.* 2017), more fundamental studies have used acoustic forcing to mimic the acoustic field with either longitudinal (Rocha *et al.* 2008; Juniper *et al.* 2009) or transverse (O'Connor 2015; Worth *et al.* 2017) forcing. Acoustic excitation enables the thorough investigation of the flame and flow behavior and has helped in understanding the mechanisms leading to CIs.

When transverse CIs occur, the acoustic field introduces transverse velocity fluctuations inside the combustion chamber and a fluctuating pressure difference between the chamber and the plenum. O'Connor *et al.* (2015) and Urbano & Selle (2017) noted that transverse fluctuations do not directly affect the heat release rate in gas turbine and liquid rocket engine configurations. However, pressure fluctuations induce longitudinal waves in burners, nozzles, and injectors, which in turn cause heat release fluctuations (Gröning *et al.* 2016; Armbruster *et al.* 2019). The acoustic response from different combustor elements is then necessary for the accurate prediction of the injector flow rate and the combustor stability. Several studies computed the injector or burner velocity fluctuations using linear acoustic models. This enabled the prediction of the combustor stability by describing the flame response with a time-lag model (Krebs *et al.* 1999) or with a numerically computed and frequency-dependent function (Krüger *et al.* 2001). The aforementioned studies, however, focused on premixed configurations. The response of non-premixed injectors to transverse acoustic waves has not been examined yet.

While there is significant literature studying the response of non-premixed flames to longitudinal acoustic forcing (e. g. Baillot & Demare 2007; Juniper *et al.* 2009; Magina *et al.* 2019), studies on non-premixed flames under transverse acoustic excitation are sparser. Plascencia *et al.* (2020) considered two forcing conditions, in which either the pressure node (PN) or the pressure anti-node (PAN) aligns with the centerplane of a non-premixed jet flame. For PN conditions, they found that the flame becomes more wrinkled but remains anchored even for a large forcing amplitude. In contrast, under a PAN mode, the flame would periodically or completely lift off and exhibit puff-like structures. By performing a large-eddy simulation (LES) of this configuration, Brouzet *et al.* (2022) showed that the acoustic response of the injectors was significant in the PAN case, resulting in large fluctuations in the mass flow rates of the fuel and oxidizer streams. This longitudinal forcing resulted in a periodically increased mixing at the stoichiometric surface, leading to significant heat release rate oscillations near the inflow. This study

focused on the physical mechanisms leading to heat release rate fluctuations but did not attempt to model the flame response.

The flame response can be modeled through Crocco's n - τ model (Crocco 1951, 1952), which correlates the integrated heat release rate to the inlet velocity fluctuations through a delayed time. This model has been applied to various premixed systems and is a simple tool to understand the main flame response characteristics. However, there are inherent limitations to this global model. For instance, the flame can be convectively non-compact, meaning that the characteristic Strouhal number based on the flame length L_f , $St = fL_f/\bar{u}$, can be much greater than unity for the frequencies of interest. This typically leads to some regions in the flame that are in phase with the acoustic field while others are out of phase, especially for a non-premixed flame with large L_f (Varoquie *et al.* 2002; Truffin 2005). This behavior weakens the thermo-acoustic coupling and contributes to the difficulties in applying the n - τ model to non-premixed flames. More complex approaches have been developed, such as flame transfer functions (Ducruix *et al.* 2000) or non-linear flame describing functions (Noiray *et al.* 2008), which can include distributed time delays (Polifke 2020). It is still unclear whether simple models like the n - τ framework can accurately describe the response of non-premixed flames and, if so, under which conditions.

This paper considers two aspects crucial to the understanding of transverse CIs in non-premixed systems: the response of the injector flow to transverse acoustic excitation and the flame response modeling. To this extent, numerical simulations of the configuration considered by Plascencia *et al.* (2020) and Brouzet *et al.* (2022) are conducted and compared against low-order models. First, the methodology of the LES is described in Section 2. Then, an analytical acoustic model for the acoustic response of the injectors is developed and compared to numerical results in Section 3. Flame response modeling is tackled in Section 4, and conclusions are presented in Section 5.

2. Methodology

2.1. Governing equations

To analyze how the acoustic field couples to the flame dynamics, LES are conducted in this work. A fully compressible finite-volume solver (Khalighi *et al.* 2011; Ma *et al.* 2017) is used to conduct the simulations. It solves the following Favre-filtered governing equations for conservation of mass, momentum, and energy,

$$\partial_t \bar{\rho} + \nabla \cdot (\bar{\rho} \tilde{\mathbf{u}}) = 0, \quad (2.1)$$

$$\partial_t (\bar{\rho} \tilde{\mathbf{u}}) + \nabla \cdot (\bar{\rho} \tilde{\mathbf{u}} \tilde{\mathbf{u}}) = -\nabla \bar{p} + \nabla \cdot \bar{\boldsymbol{\tau}}_{\nu+t}, \quad (2.2)$$

$$\partial_t (\bar{\rho} \tilde{e}_{tot}) + \nabla \cdot [\tilde{\mathbf{u}} (\bar{\rho} \tilde{e}_{tot} + \bar{p})] = \nabla \cdot (\bar{\boldsymbol{\tau}}_{\nu+t} \cdot \tilde{\mathbf{u}}) - \nabla \cdot \bar{\mathbf{q}}_{\nu+t}, \quad (2.3)$$

with density ρ , gas velocity vector $\mathbf{u} = [u, v, w]^T$, pressure p , specific total energy e_{tot} , stress tensor $\boldsymbol{\tau}$, and heat flux \mathbf{q} . Overbars and tildes denote Reynolds and Favre filtering, respectively. Subscripts ν and t denote viscous and turbulent contributions, respectively. Turbulent subgrid scales (SGS) are modeled using the Vreman model (Vreman *et al.* 2009).

The flamelet/progress-variable (FPV) approach (Pierce & Moin 2004; Ihme *et al.* 2005) is used to model the combustion process, in which the thermochemical properties are a function of the mixture fraction \tilde{Z} , the progress variable \tilde{C} , and the mixture fraction variance $\widetilde{Z'^2}$. The pressure fluctuations considered in this study do not exceed 0.5% of the

mean pressure, meaning that pressure effects on kinetics are negligible, at least compared to the other effects discussed in the paper. This is the reason why the combustion process is considered independent of pressure in the FPV approach. The solved LES equations for the quantities of interest are as follows

$$\partial_t(\bar{\rho}\tilde{Z}) + \nabla \cdot (\bar{\rho}\tilde{\mathbf{u}}\tilde{Z}) = -\nabla \cdot \bar{\mathbf{j}}_{Z,\nu+t} , \quad (2.4)$$

$$\partial_t(\bar{\rho}\tilde{C}) + \nabla \cdot (\bar{\rho}\tilde{\mathbf{u}}\tilde{C}) = -\nabla \cdot \bar{\mathbf{j}}_{C,\nu+t} + \bar{\omega}_C , \quad (2.5)$$

$$\partial_t(\bar{\rho}\tilde{Z}''^2) + \nabla \cdot (\bar{\rho}\tilde{\mathbf{u}}\tilde{Z}''^2) = -\nabla \cdot \bar{\mathbf{j}}_{Z''^2,\nu+t} . \quad (2.6)$$

The progress variable is defined as $C = Y_{\text{CO}_2} + Y_{\text{CO}} + Y_{\text{H}_2\text{O}} + Y_{\text{H}_2}$ (Ihme *et al.* 2012), and the stoichiometric mixture fraction is $Z_{st} = 0.098$. An assumed beta probability density function is used to model the subgrid fluctuations in \tilde{Z} and \tilde{C} so that the progress variable source term $\dot{\omega}_C = \dot{\omega}_C(\tilde{Z}, \tilde{C}, \tilde{Z}''^2)$. The diffusive and turbulent fluxes for the scalar Ψ are computed as $\mathbf{j}_{\Psi,\nu} = -\rho D_\Psi \nabla \Psi$ and $\mathbf{j}_{\Psi,t} = -\mu_t / Sc_t \nabla \Psi$, respectively, where D_Ψ is the diffusion coefficient, μ_t is the SGS viscosity, and Sc_t is the turbulent Schmidt number. The system is closed with the ideal gas equation of state. The chemistry model for the methane/air combustion process is described by the GRI3.0 mechanism, which consists of 53 species and 325 reactions. Constant turbulent Prandtl and Schmidt numbers of 0.7 are assumed for the scalar SGS model.

The governing equations are discretized using a hybrid scheme that combines a fourth-order accurate central spatial scheme with a second-order essentially non-oscillatory (ENO) reconstruction scheme in regions of high-density gradients (Ma *et al.* 2017). A strong stability-preserving third-order Runge-Kutta scheme is employed for time advancement with a maximum Courant-Friedrichs-Lewy number of 1.5.

2.2. Numerical setup

In the following, quantities associated with the fuel tube and the coflow annulus are denoted by subscripts f and c , respectively. The injector consists of a center tube (inner diameter $D_f = 4.0$ mm, length $L_f = 305$ mm, post thickness $w_p = 0.36$ mm) that supplies the fuel (methane). Surrounding the fuel tube is an oxidizer coflow section (outer diameter $D_c = 88.9$ mm, length $L_c = 168.4$ mm) to shield the jet from entrainment and to suppress recirculation. The oxidizer stream consists of enriched air with 40% O_2 by mass. The flow rates of the fuel and coflow streams are equal to $\dot{m}_f = 0.164$ g/s and $\dot{m}_c = 7.34$ g/s, respectively. Both streams are injected at a temperature of 293 K and at atmospheric pressure. The Reynolds number in this study ($Re = 5,300$) is evaluated at the fuel injection condition and is based on the tube exit diameter, the bulk velocity ($U_b = 25$ m/s), and the fluid properties of methane calculated at atmospheric chamber conditions.

The combustion chamber is a box of dimensions $914.4 \times 355.6 \times 108.0$ mm³. The domain considered in the LES is shown in Figure 1. A block-structured mesh with 3.9 million hexahedral elements is used, with 40 and 8 elements across the fuel tube and post-thickness wall, respectively. Boundary conditions for the speakers and the injector inlet are prescribed using a Navier-Stokes characteristic boundary condition (NSCBC) method for the injection of acoustic and vortical waves (Brouzet *et al.* 2022). While the former boundary features only incoming acoustic waves, turbulent inflow conditions are prescribed in the fuel tube. To this end, a synthetic turbulent flow is computed following the method proposed by Xie & Castro (2008) with the modifications of Touber & Sandham (2009). The mean and root mean square profiles at an equivalent Reynolds

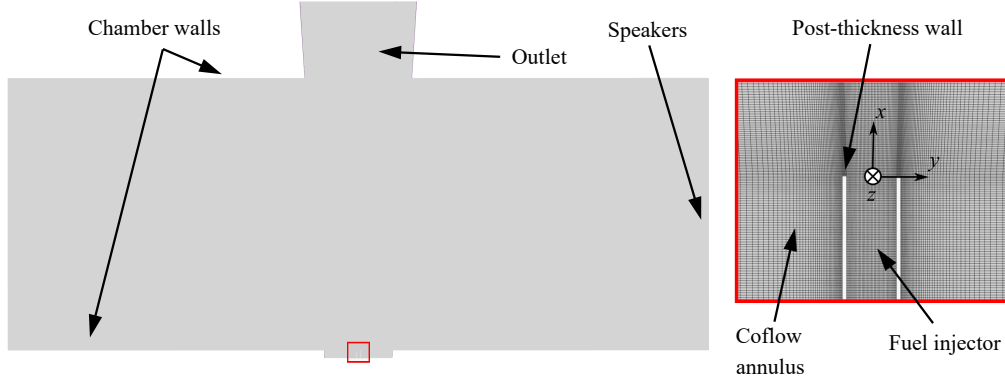


Figure 1: Two-dimensional schematic of the domain considered in the LES.

number are used to define the fully developed pipe flow characteristics using an integral length scale of $0.3D_f$. The outlet is modeled by a non-reflecting NSCBC with a relaxation timescale of the order of 15 ms. A damping region, which relaxes the solution to a target, fully combusted, equilibrium state, is used in the exhaust section of the domain. This damping region prevents any thermodynamic or chemical inhomogeneities at the outlet that would lead to a spurious behavior with the non-reflecting locally one-dimensional and inviscid boundary conditions. To this end, the formulation developed by Bogey *et al.* (2000) is used, combined with a linear relaxation factor in the streamwise direction.

Two simulations were conducted in this work. The first one was performed to study the acoustic response of the injectors to a transverse acoustic mode by considering the whole injector length. The mixture is not ignited in this case, and the results are compared to a low-order theoretical acoustic model. The second simulation is an LES of the flame, where the injector's boundary conditions were specified using the derived acoustic model with a reduced injector length, as shown in Figure 1. In both simulations, the acoustic waves are prescribed from the two transverse boundaries, which model the speakers. For both simulations, a transverse acoustic forcing is performed for the first PAN mode (i.e., at $f = 360$ Hz); therefore the waves injected at both ends are in phase, leading to a zero transverse velocity amplitude at the injector exit.

3. Acoustic response of the injector

In this section, we develop an analytical model to describe the acoustic response of the coaxial injector to transverse acoustic waves in the chamber. The following analysis assumes that the acoustic wavelength, λ , is large compared to the injector diameters, so that only planar waves are present. The most restrictive condition is therefore imposed by the coflow diameter $D_c/\lambda \leq 0.61$ (Levine & Schwinger 1947), providing a constraint for the frequency of $f \leq 0.61c/D_c \simeq 2350$ Hz, with c being the speed of sound in the injector. Then, the pressure and streamwise velocity fluctuations in the injector can be written as a function of the upstream and downstream propagating acoustic wave amplitudes A^-

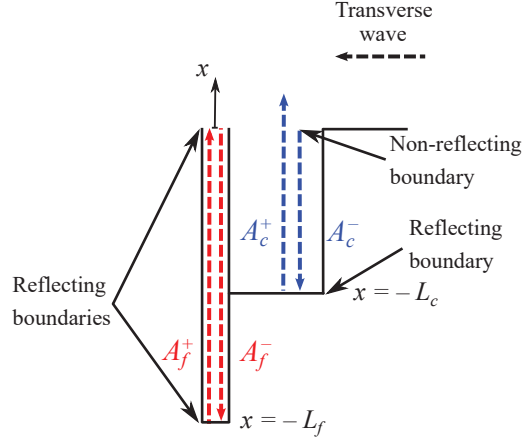


Figure 2: Schematic of the acoustic waves in the coaxial injector. The blue and red dashed arrows represent the waves in the coflow annulus and jet tube, respectively.

and A^+ , respectively,

$$p'(x, t) = \Re \{ [A^+ \exp(jkx) + A^- \exp(-jkx)] \exp(-j\omega t) \} , \quad (3.1a)$$

$$u'(x, t) = \frac{1}{\rho c} \Re \{ [A^+ \exp(jkx) - A^- \exp(-jkx)] \exp(-j\omega t) \} , \quad (3.1b)$$

where j represents the imaginary unit, $k = 2\pi f/c$ is the wavenumber, $\omega = 2\pi f$ is the angular frequency, and $\Re \{ \cdot \}$ means that only the real part is considered.

We first consider the response of the coflow. The transverse waves generated by the speakers will diffract in the coflow annulus, leading to an upstream propagating wave of amplitude $A_c^- = \Delta p$, equal to the combined amplitudes of the two transverse waves in the chamber. As the boundary condition at the bottom of the annulus $x = -L_c$ is fully reflective, an upstream propagating wave of amplitude A_c^+ will be created. A schematic of the waves is shown in Figure 2. Solving Eq. (3.1) by applying the wall boundary condition $u'_c(-L_c, t) = 0$ leads to the following solution at the coflow exit

$$p'_c(0, t) = \Delta p \Re \{ [\exp(2jkL_c) + 1] \exp(-j\omega t) \} , \quad (3.2a)$$

$$u'_c(0, t) = \frac{\Delta p}{\rho c} \Re \{ [\exp(2jkL_c) - 1] \exp(-j\omega t) \} . \quad (3.2b)$$

Equations (3.2a)-(3.2b) show that the pressure and velocity at the coflow annulus exit have an amplitude and phase difference relative to the incoming transverse waves, which is a function of the annulus length L_c .

The downstream propagating wave will then diffract into the combustion chamber, with negligible reflection back into the coflow annulus. Considering our model, this means that the pressure at the fuel nozzle is imposed by Eq. (3.2a), which can be written as

$$p'_f(0, t) = \Delta p_f \Re \{ \exp(-j\omega t + \phi) \} , \quad (3.3)$$

where $\Delta p_f = \max[p'_c(0, t)]$ and ϕ are the amplitude and phase of the pressure fluctuations. The condition of zero pressure differential across the nozzle is a well-known result for sharp-edge open pipes with small diameters (Van Wijngaarden 1968). While the coflow outlet is large compared to the acoustic wavelength, the fuel tube diameter

is much smaller, explaining the non-reflective and fully reflective behavior of the coflow and fuel tube outlets, respectively. In the fuel tube, we have an acoustic problem with the two following boundary conditions: The upstream propagating wave with amplitude A_f^- is reflected at $x = -L_f$ by the upstream choked flow condition, and the downstream propagating wave with amplitude A_f^+ is reflected by the imposed harmonic pressure condition at the fuel tube outlet (Eq. (3.3)). To analytically solve this problem of reflected waves both at the bottom and at the top of the fuel tube, the method of characteristics is used (Rienstra & Hirschberg 2004). This method leads to the following solution for the downstream and upstream propagating waves

$$A_f^- = \Delta p_f \Re \left\{ \sum_{n=0}^{N_1} (-1)^n \exp(2jknL_f) \right\}, \quad (3.4a)$$

$$A_f^+ = -\Delta p_f \Re \left\{ \sum_{n=1}^{N_2} (-1)^n \exp(2jknL_f) \right\}, \quad (3.4b)$$

where the integers $N_1 = \lfloor (ct + x)/2L_f \rfloor$ and $N_2 = \lfloor (ct - x)/2L_f \rfloor$ act as counters for the reflected waves. Knowing the analytical form of the geometric series, one can combine Eqs. (3.1b)-(3.4) to express the velocity fluctuations at the fuel tube outlet

$$u'_f(0, t) = -\frac{\Delta p_f}{\rho c} \Re \left\{ \left[\frac{1 + (-1)^N \exp[2jk(N+1)L_f]}{1 + \exp(2jkL_f)} + \exp(2jkL_f) \frac{-1 + (-1)^N \exp(2jkNL_f)}{1 + \exp(2jkL_f)} \right] \exp(-j\omega t + \phi) \right\}, \quad (3.5a)$$

where $N = N_1 = N_2$ and the pressure fluctuations at this location are computed from Eq. (3.3).

To assess this analytical model, Figure 3 shows comparisons of the pressure fluctuations inside the fuel tube and the coflow between the simulation and the model. Substantial pressure fluctuations are observed inside the injector, and the interaction of the acoustic waves within the injector leads to pressure fluctuations that are much higher at the bottom of the fuel tube than inside the chamber. The good agreement between the simulation and analytical model suggests that the behavior of the acoustic waves is physical.

Velocity fluctuations obtained at the exits of the coflow annulus and the fuel tube are shown in Figure 4, as a function of the normalized time $t_f = ft$. The fuel tube velocity signal features an acoustic beating mode, resulting from the superposition of the forcing frequency and the first resonant frequency of the fuel tube $f_1 = c/(4L_f) \simeq 280$ Hz. This result confirms that the exit of the tube acts as a reflecting interface for the acoustic waves and that losses are negligible, as assumed in the model and supported by the theory of Levine & Schwinger (1947) that predicts a near-unity reflection coefficient for the frequency and tube diameter considered. In contrast, the coflow signal is quasi-harmonic at the forcing frequency of $f = 360$ Hz, showing that the open end of the annulus is nearly non-reflecting.

To further assess the analytical model, Eqs. (3.2b)-(3.5a) are compared to the simulation results in Figure 4. Amplitude and phase are in good agreement for the coflow. In addition, the beating behavior in the fuel tube is well captured by the analytical model, especially when the velocity fluctuations are maximum. Overall, these results show that

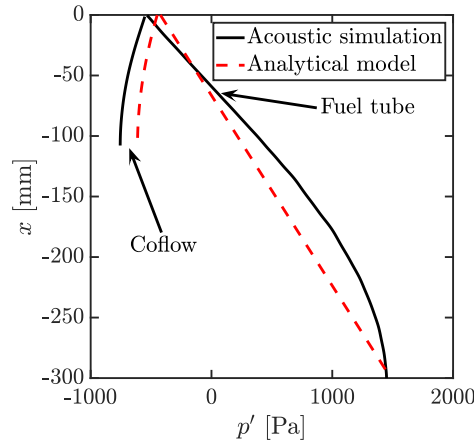


Figure 3: Pressure fluctuations inside the injector obtained with the acoustic simulations and the analytical model.

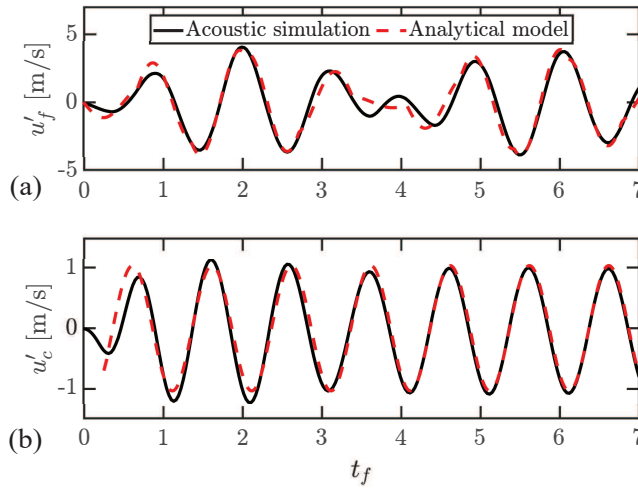


Figure 4: Velocity fluctuations at the exit of (a) the fuel tube and (b) the coflow obtained with the acoustic simulations and the analytical model.

the acoustic behavior in the fuel tube is well represented by linear acoustics with a perfectly reflecting open end and negligible losses.

4. Flame response modeling

We proceed by briefly explaining the flame dynamics resulting from the acoustic forcing. Figure 5 shows an instantaneous snapshot of the flame. The temperature field at the x - y centerplane displays puff-like characteristics. The horizontal streaks identified around $x/D_f = 9$ in the coflow region arise from the initialization process, and are slowly convected downstream. While clearly identifiable, they are not significantly contributing to

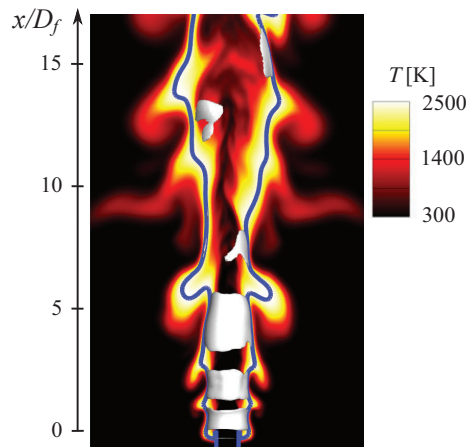


Figure 5: Instantaneous snapshot of the flame. The color plot represents the temperature field, the isolines show $Z_{st} = 0.098$, and the isosurfaces show $\dot{Q} = 5 \text{ GW/m}^3$.

the heat released by the flame. The isoline indicates the stoichiometric contour with $Z_{st} = 0.098$, which is substantially corrugated by the surrounding flow field in the first ten jet diameters downstream of the inlet. The regions with heat release rate larger than $\dot{Q} = 5 \text{ GW/m}^3$ are shown by the white isosurfaces and tend to be located in the lower part of the flame. Brouzet *et al.* (2022) performed an in-depth study of the flow, mixing and flame dynamics. To summarize their findings, vortices in the outer shear layer arising from the coflow forcing corrugate the flame in the near-nozzle region. Simultaneously, the jet longitudinal forcing enhances the mixing at greater radial locations. The combination of these two mechanisms periodically increases the heat release rate where the flame is close enough to the centerline. Hence, the longitudinal fluctuations in the coflow and the jet play complementary roles, leading to substantial heat release rate oscillations in the near-inflow region.

In order to examine the coupling between the inlet fluctuations and the heat release, we proceed by analyzing the associated heat release rate fluctuations. Figure 6(a) shows the inlet mass flow rate and integrated heat release rate fluctuations in the flame region up to $x/D_f = 25$. Strong mass flow and heat release rate oscillations, of the order of 40% and 5% of their nominal values, respectively, are observed. The amount of fuel burned, i.e., the heat release rate average, remained the same whether the flame was excited or not. The relative lower fluctuations of the heat release rate compared to the mass flow fluctuations are only an indication of the flame response strength. The coupling between the pressure at the flame location and $\dot{\Omega}'$ is shown in Figure 6(b). Both signals are almost in phase even though some low-frequency behavior can be seen for $\dot{\Omega}'$ and can be attributed to the slow flame convection in the shear layer.

Figure 6 implies a coupling between the jet forcing and the flame response. To quantify this response and to evaluate the utility of a simple model in describing the observed dynamics, we employ Crocco's n - τ model (Crocco 1951, 1952). This model expresses the global heat release rate fluctuations $\dot{\Omega}'(t)$ as a function of the inlet mass flow rate fluctuation \dot{m}' at a delayed time τ ,

$$\frac{\gamma - 1}{c^2} \dot{\Omega}'(t) = \dot{m}'(t - \tau)n, \quad (4.1)$$

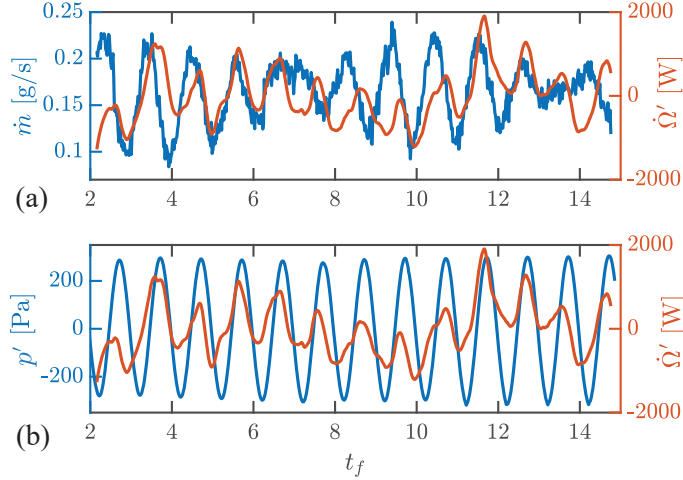


Figure 6: Time signals of the integrated heat release rate fluctuations $\dot{\Omega}'$ compared to (a) the inlet mass flow rate \dot{m} and (b) the pressure fluctuations p' in the flame region.

where n represents the interaction coefficient (i.e., the strength of the flame response) and τ is a measure of the time required by the flame to respond to forcing. The thermodynamic properties are taken at the fuel inlet. Equation (4.1) implies that all reactants are consumed at a specific time τ after their injection, suggesting that the flame is convectively compact. This can be a strong assumption for non-premixed flames given that mixing and diffusion play a dominant role in the combustion process. A convectively non-compact version of Crocco's model can be written by considering a streamwise dependence of the model parameters (Varoquie *et al.* 2002; Truffin 2005)

$$\frac{\gamma - 1}{c^2} \int_{x-\Delta x/2}^{x+\Delta x/2} \dot{Q}'(x, t) dx = \dot{m}'(t - \tau_x) n_x, \quad (4.2)$$

where τ_x and n_x are dependent on the streamwise position. The streamwise interval Δx over which the integral is performed is set to $4D_f$ in this study, which was found to give converged results.

To compute the n - τ parameters, a methodology analogous to the one described by Frezzotti *et al.* (2018) is used. To this end, the normalized cross-correlation $R_{\dot{m}\dot{\Omega},norm}$ between \dot{m}' and $\dot{\Omega}'$ is computed for a range of time delays. The time delay at which $R_{\dot{m}\dot{\Omega},norm}$ is maximum is then defined as the optimum τ in Crocco's model. The interaction coefficient n is then evaluated by minimizing the function $|(\gamma - 1)\dot{\Omega}'(t)/c^2 - \dot{m}'(t - \tau)n|$. Results from this methodology are shown in Figure 7(a), which shows the cross-correlation and interaction parameters for a range of time delays. The cross-correlation is quasi-periodic given the oscillatory nature of the flow. The vertical dashed lines represent the time delays $\tau_1 = 0.16/f$ and $\tau_2 = 1.18/f$ associated with the first two peaks of $R_{\dot{m}\dot{\Omega},norm}$, which have comparable amplitudes. The corresponding interaction coefficients are $n \simeq 15$. Figure 7(b) shows results for the non-compact model. To remove the low-frequency oscillations, a high-pass filter with a cutoff frequency of 270 Hz was applied to the heat

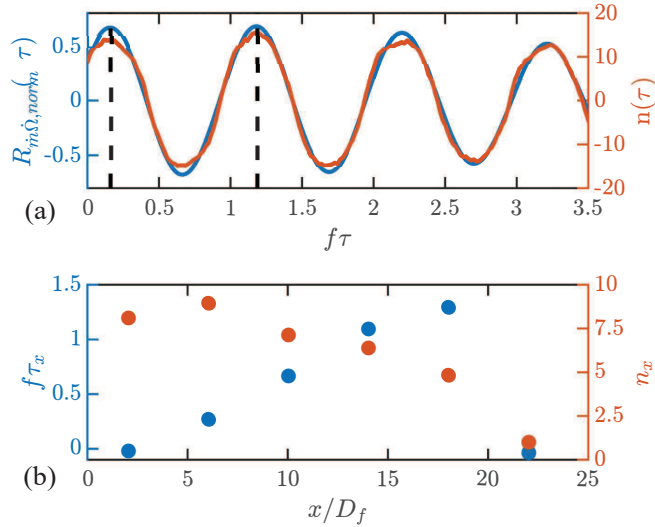


Figure 7: Estimation of n - τ parameters for (a) the compact model (Eq. (4.1)) and (b) the non-compact model (Eq. (4.2)).

release rate signals. The time delay follows an almost linear behavior. The interaction coefficient peaks at $x/D_f \approx 5$, which corresponds to the delay time τ_1 in the compact model. In the region $x/D_f > 15$, n_x gradually decreases, which is consistent with the weaker mixing interaction observed in that region (Brouzet & Ihme 2021; Brouzet *et al.* 2022). For $x/D_f > 20$, the cross-correlation is so low that the methodology fails to find a physically meaningful time delay.

At this point, it is interesting to note that the interaction coefficients identified with the compact and non-compact models are up to two orders of magnitude larger than those of previous non-premixed flame studies for propane flames in a coaxial slot injector at comparable operating conditions (Varoquie *et al.* 2002; Truffin 2005). The difference might be explained by the sole forcing of the air inlet in these studies, which was found to weakly alter the heat release rate and only at large downstream locations. In contrast, the highest values of n_x are identified close to the inflow in our case. For comparison with previous flame transfer function studies, it is useful to rewrite Eq. (4.1) as

$$\frac{\dot{\Omega}'(t)}{\bar{\Omega}} = F_n \frac{u'(t - \tau)}{U_b}, \quad (4.3)$$

where $\bar{\Omega} = 12$ kW and $U_b = 25$ m/s, which yields a value $F_n \simeq 0.15$. This value is on par with the ones obtained for similar chamber and fuel conditions for premixed laminar lean Bunsen-type flames (Duchaine *et al.* 2011; Silva *et al.* 2015) at the frequency studied in this paper. Interestingly, these laminar flames were subjected to intrinsic thermo-acoustic instabilities at lower frequencies.

To conclude, we construct a global model for the flame response by estimating the fuel flow rate fluctuations from the acoustic model defined in Section 3 and computing the flame response from Crocco's model. Both the convectively compact and non-compact formulations of Crocco's model are considered to estimate the effect of the compactness

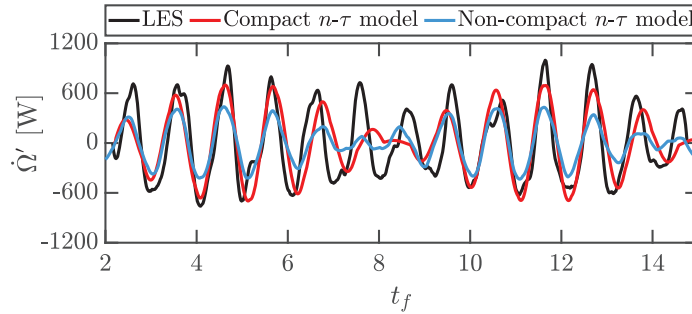


Figure 8: Comparison of the integrated heat release rate fluctuations $\dot{\Omega}'$ between the LES results, the compact n - τ model (Eq. (4.1)), and the non-compact n - τ model (Eq. 4.2)).

assumption. A comparison between the LES and model results is shown in Figure 8. Effects due to turbulence or flame corrugation are not taken into account and contribute to the discrepancies observed between the LES and the models. Even so, the maximum amplitude and frequency of the heat release rate fluctuations are reasonably well predicted. The convectively compact model performs at least as well as the non-compact one, illustrating that the former is well suited for the non-premixed system studied. Because the strong heat release rate oscillations are limited to a region close to the inflow, the underlying assumptions that the combustion is correlated to the fuel flow rate and that it occurs at a specific delayed time are both satisfied. Overall, these results show that a modeling strategy combining the acoustic response of the injector and Crocco's model for the flame response can lead to a reasonable prediction of non-premixed flame dynamics. The strength of the global model which combines the acoustic response of the injector and Crocco's approach is that, for a given flame response (i.e., τ and n values), one can investigate the effect of different injector parameters (e.g., injector length, upstream boundary conditions, presence of a coflow annulus) on the overall flame response.

5. Conclusions

A turbulent non-premixed methane/air flame under a transverse acoustic mode was studied to assess low-order models. The flame was subjected to a standing PAN wave, where pressure oscillations are maximum at the centerline. Using this configuration, we studied two important aspects related to transverse CIs: the acoustic response of the injector and the flame response modeling.

Acoustic simulations revealed that transverse acoustic modes introduce strong longitudinal velocity perturbations in the injector, both in the coflow and in the fuel jet. An analytical model was developed to predict the acoustic fluctuations in the injector, showing good agreement with simulation results and implying that the acoustic behavior in the fuel tube is well represented by linear acoustics with a perfectly reflecting open end and negligible losses.

Substantial heat release rate oscillations in the near-inflow region were observed in the LES. Modeling using both convectively compact and non-compact n - τ models showed that the flame response was strong for a non-premixed configuration. A global model combining the acoustic and compact n - τ models showed good agreement with LES results. Because the large heat release rate fluctuations were limited to a region close to the inflow, the underlying assumptions that the combustion is correlated to the fuel flow

rate and that it occurs at a specific delayed time were both satisfied. This study showed that a modeling strategy combining the acoustic response of the injector and Crocco's model for the flame response can lead to a reasonable prediction of non-premixed flame dynamics.

Acknowledgments

Financial support through the Air Force Research Laboratory (award # RAPF1-0000001326), the Air Force Office for Scientific Research (award # FA9550-21-1-0077), and the Ohio Aerospace Institute is gratefully acknowledged. The computational resources supporting this work are provided by the National Energy Research Scientific Computing Center.

REFERENCES

- ARMBRUSTER, W., HARDI, J. S., SUSLOV, D. & OSCHWALD, M. 2019 Injector-driven flame dynamics in a high-pressure multi-element oxygen–hydrogen rocket thrust chamber. *J. Propul. Power* **35**, 632–644.
- BAILLOT, F. & DEMARE, D. 2007 Responses of a lifted non-premixed flame to acoustic forcing. Part 2. *Combust. Sci. Technol.* **179**, 905–932.
- BOGEY, C., BAILLY, C. & JUVE, D. 2000 Numerical simulation of sound generated by vortex pairing in a mixing layer. *AIAA J.* **38**, 2210–2218.
- BROUZET, D., YOU, S., PLASCENCIA, M. A., ROA, M. & IHME, M. 2022 The dynamics of non-premixed flames subjected to a transverse acoustic mode. *Combust. Flame* **246**, 112330.
- BROUZET, D. & IHME, M. 2021 Flame dynamics of a non-premixed turbulent flame under transverse acoustic forcing. *Annual Research Briefs*, Center for Turbulence Research, Stanford University, pp. 143–152.
- CROCCO, L. 1951 Aspects of combustion stability in liquid propellant rocket motors. Part I: Fundamentals. Low frequency instability with monopropellants. *J. Am. Rocket Soc.* **21**, 163–178.
- CROCCO, L. 1952 Aspects of combustion stability in liquid propellant rocket motors. Part II: Low frequency instability with bipropellants. High frequency instability. *J. Am. Rocket Soc.* **22**, 7–16.
- DUCHAINE, F., BOUDY, F., DUROX, D. & POINSOT, T. 2011 Sensitivity analysis of transfer functions of laminar flames. *Combust. Flame* **158**, 2384–2394.
- DUCRUIX, S., DUROX, D. & CANDEL, S. 2000 Theoretical and experimental determinations of the transfer function of a laminar premixed flame. *P. Combust. Inst.* **28**, 765–773.
- FREZZOTTI, M. L., NASUTI, F., HUANG, C., MERKLE, C. L. & ANDERSON, W. E. 2018 Quasi-1D modeling of heat release for the study of longitudinal combustion instability. *Aerosp. Sci. Technol.* **75**, 261–270.
- GRÖNING, S., HARDI, J. S., SUSLOV, D. & OSCHWALD, M. 2016 Injector-driven combustion instabilities in a hydrogen/oxygen rocket combustor. *J. Propul. Power* **32**, 560–573.
- IHME, M., CHA, C. M. & PITSCH, H. 2005 Prediction of local extinction and re-ignition effects in non-premixed turbulent combustion using a flamelet/progress variable approach. *P. Combust. Inst.* **30**, 793–800.
- IHME, M., SHUNN, L. & ZHANG, J. 2012 Regularization of reaction progress variable for application to flamelet-based combustion models. *J. Comput. Phys.* **231**, 7715–7721.

- JUNIPER, M. P., LI, L. K. B. & NICHOLS, J. W. 2009 Forcing of self-excited round jet diffusion flames. *P. Combust. Inst.* **32**, 1191–1198.
- KHALIGHI, Y., HAM, F., NICHOLS, J., LELE, S. & MOIN, P. 2011 Unstructured large eddy simulation for prediction of noise issued from turbulent jets in various configurations. *AIAA Paper* 2011-2886.
- KREBS, W., WALZ, G. & HOFFMANN, S. 1999 Thermoacoustic analysis of annular combustor. *AIAA Paper* 1999-1971.
- KRÜGER, U., HÜREN, J., HOFFMANN, S., KREBS, W., FLOHR, P. & BOHN, D. 2001 Prediction and measurement of thermoacoustic improvements in gas turbines with annular combustion systems. *J. Eng. Gas Turb. Power* **123**, 557–566.
- LEVINE, H. & SCHWINGER, J. 1947 On the radiation of sound from an unflanged circular pipe. *Phys. Rev.* **73**, 383–406.
- LIEUWEN, T. & YANG, V., ed. 2005 *Combustion instabilities in gas turbine engines: operational experience, fundamental mechanisms and modeling*. American Institute of Aeronautics and Astronautics.
- MA, P. C., LV, Y. & IHME, M. 2017 An entropy-stable hybrid scheme for simulations of transcritical real-fluid flows. *J. Comput. Phys.* **340**, 330–357.
- MAGINA, N., ACHARYA, V. & LIEUWEN, T. 2019 Forced response of laminar non-premixed jet flames. *Prog. Energ. Combust.* **70**, 89–118.
- NOIRAY, N., DUROX, D., SCHULLER, T. & CANDEL, S. 2008 A unified framework for nonlinear combustion instability analysis based on the flame describing function. *J. Fluid Mech.* **615**, 139–167.
- O’CONNOR, J. 2015 Visualization of shear layer dynamics in a transversely forced flow and flame. *J. Propul. Power* **31**, 1127–1136.
- O’CONNOR, J., ACHARYA, V. & LIEUWEN, T. 2015 Transverse combustion instabilities: acoustic, fluid mechanic, and flame processes. *Prog. Energ. Combust.* **49**, 1–39.
- PIERCE, C. D. & MOIN, P. 2004 Progress-variable approach for large-eddy simulation of non-premixed turbulent combustion. *J. Fluid Mech.* **504**, 73–97.
- PLASCENCIA, M., ROA, M., KARAGOZIAN, A. & TALLEY, D. G. 2020 Turbulent non-premixed jet flames under transverse acoustic forcing. *AIAA Paper* 2020-3805.
- POLIFKE, W. 2020 Modeling and analysis of premixed flame dynamics by means of distributed time delays. *Prog. Energ. Combust.* **79**, 100845.
- PRIEUR, K., DUROX, D., SCHULLER, T. & CANDEL, S. 2017 A hysteresis phenomenon leading to spinning or standing azimuthal instabilities in an annular combustor. *Combust. Flame* **175**, 283–291.
- RIENSTRA, S. W. & HIRSCHBERG, A. 2004 *An introduction to acoustics*. Eindhoven University of Technology.
- ROCHA, A. M. A., CARVALHO, J. A. & LACAVA, P. T. 2008 Gas concentration and temperature in acoustically excited Delft turbulent jet flames. *Fuel* **87**, 3433–3444.
- ROUWENHORST, D., HERMANN, J. & POLIFKE, W. 2017 Online monitoring of thermoacoustic eigenmodes in annular combustion systems based on a state-space model. *J. Eng. Gas Turb. Power* **139**, 021502.
- SILVA, C. F., EMMERT, T., JAENSCH, S. & POLIFKE, W. 2015 Numerical study on intrinsic thermoacoustic instability of a laminar premixed flame. *Combust. Flame* **162**, 3370–3378.
- TOUBER, E. & SANDHAM, N. D. 2009 Large-eddy simulation of low-frequency unsteady-

- ness in a turbulent shock-induced separation bubble. *Theor. Comp. Fluid Dyn.* **23**, 79–107.
- TRUFFIN, K. 2005 Simulations aux grandes échelles et identification acoustique des turbines à gaz en régime partiellement prémélangé. PhD thesis, Institut National Polytechnique de Toulouse.
- URBANO, A. & SELLE, L. 2017 Driving and damping mechanisms for transverse combustion instabilities in liquid rocket engines. *J. Fluid Mech.* **820**, R2.
- VAN WIJNGAARDEN, L. 1968 On the oscillations near and at resonance in open pipes. *J. Eng. Math.* **2**, 225–240.
- VAROQUIE, B., LEGIER, J. P., LACAS, F., VEYNANTE, D. & POINSOT, T. 2002 Experimental analysis and large eddy simulation to determine the response of non-premixed flames submitted to acoustic forcing. *P. Combust. Inst.* **29**, 1965–1970.
- VREMAN, A. W., VAN OIJEN, J. A., DE GOEY, L. P. H. & BASTIAANS, R. J. M. 2009 Subgrid scale modeling in large-eddy simulation of turbulent combustion using premixed flamelet chemistry. *Flow Turbul. Combust.* **82**, 511–535.
- WOLF, P., STAFFELBACH, G., GICQUEL, L., MÜLLER, J. D. & POINSOT, T. 2012 Acoustic and large eddy simulation studies of azimuthal modes in annular combustion chambers. *Combust. Flame* **159**, 3398–3413.
- WORTH, N. A., DAWSON, J. R., SIDEY, J. A. & MASTORAKOS, E. 2017 Azimuthally forced flames in an annular combustor. *P. Combust. Inst.* **36**, 3783–3790.
- XIE, Z. T. & CASTRO, I. P. 2008 Efficient generation of inflow conditions for large eddy simulation of street-scale flows. *Flow Turbul. Combust.* **81**, 449–470.